J. Fluid Mech. (2006), *vol.* 566, *pp.* 465–475.
doi:10.1017/S0022112006002096 Printed in the United Kingdom

Motion of a spherical particle in film flow

By C. POZRIKIDIS

Department of Mechanical and Aerospace Engineering, University of California, San Diego, La Jolla, California 92093-0411, USA

(Received 21 May 2006 and in revised form 13 July 2006)

The motion of a spherical particle suspended in gravity-driven film flow down an inclined plane is considered in the limit of vanishing Reynolds and Bond numbers where the free-surface deformation is infinitesimal. Taking advantage of the axially symmetry of the boundaries of the flow with respect to the axis that is normal to the wall and free surface and passes through the particle centre, the problem is formulated as a system of one-dimensional integral equations for the first Fourier coefficients of the unknown traction and velocity along the boundary contours in a meridional plane. It is found that the particle translational velocity scaled by the unperturbed velocity evaluated at the particle centre increases monotonically as the particle approaches the free-surface, whereas the corresponding angular velocity of rotation scaled by the unperturbed vorticity evaluated at the particle centre reaches a maximum at a certain intermediate position. The free-surface velocity vector field and deformation are displayed, the force and torque exerted on a spherical particle adhering to the wall are tabulated, and the associated flow pattern is discussed.

1. Introduction

Particle motion in a viscous fluid has been the subject of numerous studies because of its significance in a variety of disciplines ranging from the rheology of particulate media, to biofluid-dynamics of blood flow, and to microfluidics transport. Though the effect of planar and cylindrical boundaries representing confining surfaces has been documented for several flow configurations, the simultaneous effect of a boundary and a free-surface occurring in gravity-driven film flow remains poorly resolved. Li & Pozrikidis (2002, 2003) performed simulations of the film flow of an idealized two-dimensional suspension of liquid droplets and rigid particles and found that the collective interaction leads to particle migration away from the wall and the free-surface. Loimer, Nir & Semiat (2002) and Singh, Nir & Semiat (2006) studied the topography of a free-surface confining a concentrated suspension in a Couette or gravity-driven flow device and documented the effect of the particle size, concentration, and surface tension. Most relevant is the work of Timberlake & Morris (2005) who conducted a laboratory investigation of the film flow of a concentrated suspension of neutrally buoyant spherical particles down an inclined plane and demonstrated the severe rippling of the free-surface. Timberlake & Morris found that conventional suspension models are unable to describe all features of the film flow, especially those pertaining to the particle concentration distribution across the film thickness. The laboratory observations have revealed a variety of flow structures and geometrical patterns including 'surface turbulence' induced by particle clusters. Other authors have considered the deformation of the film surface down an inclined wall over a

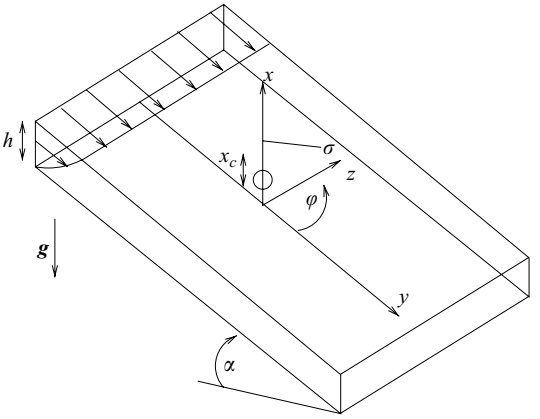

FIGURE 1. Illustration of gravity-driven flow of a liquid film down an inclined plane in the presence of a freely suspended or fixed spherical particle.

fabricated wall topography, irregularity, or a small particle arrested on the wall (e.g. Blyth & Pozrikidis 2006).

In this paper, we consider the most elementary problem of particulate film flow concerning the motion of an isolated spherical particle under conditions of Stokes flow. The main objective is to compute the particle velocity of translation and angular velocity of rotation in the limit of small Bond number where the surface deformation is small and can be considered infinitesimal. Accurate computations will become feasible by exploiting the axially symmetry of the domain of flow in order to simplify the boundary integral representation of this inherently three-dimensional flow. The reduction yields a system of one-dimensional integral equations for the first Fourier coefficients of the boundary traction and free-surface velocity defined over three boundary contours in an azimuthal plane. Numerical solutions may then be computed accurately and efficiently by elementary numerical methods. A similar reduction has been used previously to compute flow past solid surfaces with axisymmetric irregularities in the form of a particle, a depression, or a protrusion (Pozrikidis 1994*a*, *b*, 1997, 2000; Matzen 1997; Shatz 2004). After the integral equations have been solved, the free-surface deformation can be reconstructed to leading order with respect to the Bond number. As a complement to the main problem of free particle motion, the force and torque exerted on a particle adhering to the wall are computed at a minimal cost, and the free-surface velocity field and deformation are illustrated.

2. Problem statement and formulation

We consider the steady gravity-driven flow of a liquid film down an inclined plane wall in the presence of a suspended spherical particle of radius a that executes rigid-body motion, as illustrated in figure 1. In the inclined system of Cartesian coordinates depicted, the x-axis is perpendicular to the wall and passes through the particle centre, and the y-axis is parallel to the projection of the gravitational acceleration vector on the wall. Far from the particle, we obtain unidirectional flow with a flat surface described by the Nusselt solution, designated by the superscript ∞. The far-field velocity and pressure profiles, $u_x^\infty = 0$, $u_z^\infty = 0$,

$$u_y^\infty = \frac{\rho g \sin\alpha}{2\mu} x\,(2h - x), \qquad p^\infty = P_A + \rho g \cos\alpha\,(h - x), \tag{2.1}$$

for $0 \leqslant x \leqslant h$, satisfy the condition of zero velocity on the wall, zero shear stress at the film surface, and uniform normal stress at the film surface, where ρ is the fluid density, μ is the fluid viscosity, g is the acceleration due to gravity, α is the plane inclination angle, h is the film thickness, and P_A is the ambient pressure. The free-surface velocity is $U_s = u_y^{\infty}(y=h) = \rho g \sin\alpha h^2/(2\mu)$.

The particle generates a disturbance flow, denoted by the superscript D, that may be added to the unidirectional Nusselt flow to yield the total flow with velocity $\boldsymbol{u} = \boldsymbol{u}^{\infty} + \boldsymbol{u}^{D}$ and pressure $p = p^{\infty} + p^{D}$. Since no assumption is made regarding the particle size, the disturbance and unpertubed flows are of the same order of magnitude. The no-slip and no-penetration boundary conditions require $\boldsymbol{u} = \boldsymbol{0}$ over the wall and $\boldsymbol{u} = \boldsymbol{V} + \boldsymbol{\Omega} \times (\boldsymbol{x} - \boldsymbol{x}_c)$ over the particle surface, where $\boldsymbol{V}$ is the velocity of translation of the particle centre, $\boldsymbol{x}_c = (x_c, 0, 0)$, and $\boldsymbol{\Omega}$ is the angular velocity of rotation about $\boldsymbol{x}_c$. Kinematic compatibility over the free-surface requires $\boldsymbol{u} \cdot \boldsymbol{n} = 0$, where $\boldsymbol{n}$ is the unit normal vector pointing into the film. In the absence of surfactants, the shear stress is required to vanish over the free-surface, $\boldsymbol{n} \times \boldsymbol{f} \times \boldsymbol{n} = \boldsymbol{0}$, and the normal stress is balanced by surface tension, $\boldsymbol{f} \cdot \boldsymbol{n} = P_A + \gamma 2\kappa_m$ where $\boldsymbol{f} \equiv \boldsymbol{\sigma} \cdot \boldsymbol{n}$ is the traction, $\boldsymbol{\sigma}$ is the stress tensor, γ is the surface tension, κ_m is the mean curvature given by $\kappa_m = \frac{1}{2} \nabla_s \cdot \boldsymbol{n}$, and ∇_s is the surface gradient.

We will assume that the surface tension is so strong that the deformation of the free-surface from the undisturbed flat shape is infinitesimal. The formal condition is that the Bond number, $Bo = \mu U_s/\gamma$, is sufficiently small. Describing the free-surface as $x = h[1 + Bo\phi(y, z)]$, where ϕ is a dimensionless shape function, inserting into the above free-surface kinematic and dynamic conditions, shifting the location of the boundary conditions to the undeformed free-surface, and linearizing with respect to Bo, we find that, to zeroth order, the x velocity component and the y and z components of the disturbance traction are zero at $x = h$. The kinematic condition replaces the usual dynamic condition requiring that the normal component of the traction be balanced by the capillary force due to surface tension.

The Reynolds number written with respect to the particle size is assumed to be so small that the motion of the fluid is governed by the equations of Stokes flow written here for the disturbance flow, $-\nabla p^D + \mu \nabla^2 \boldsymbol{u}^D = \boldsymbol{0}$, and $\nabla \cdot \boldsymbol{u}^D = 0$. The body force due to gravity has been absorbed in the parabolic velocity profile and linear pressure profile of the unidirectional Nusselt flow. To compute the solution, we use the boundary integral formulation for Stokes flow and express the disturbance velocity in terms of integrals over the wall, W, the film surface F, and the particle surface, P:

$$\boldsymbol{u}^D(\boldsymbol{x}_0) = -\frac{1}{8\pi\mu}\mathscr{S}(\boldsymbol{x}_0, \boldsymbol{f}, P) - \frac{1}{8\pi\mu}\mathscr{S}(\boldsymbol{x}_0, \boldsymbol{f}^D, WF) + \frac{1}{8\pi}\mathscr{D}(\boldsymbol{x}_0, \mathbf{u}^D, F), \tag{2.2}$$

where the point $\boldsymbol{x}_0$ lies in the fluid. We have introduced the single- and double-layer potentials of Stokes flow defined over a generic surface, D:

$$\left.\begin{aligned} \mathscr{S}_j(\boldsymbol{x}_0, \boldsymbol{f}, D) &\equiv \iint_D f_i(\boldsymbol{x}) G_{ij}(\boldsymbol{x}, \boldsymbol{x}_0)\, \mathrm{d}S(\boldsymbol{x}), \\ \mathscr{D}_j(\boldsymbol{x}_0, \boldsymbol{u}, D) &\equiv \iint_D u_i(\boldsymbol{x}) T_{ijk}(\boldsymbol{x}, \boldsymbol{x}_0) n_k(\boldsymbol{x})\, \mathrm{d}S(\boldsymbol{x}), \end{aligned}\right\} \tag{2.3}$$

where $\mathrm{d}S$ is a differential surface area

$$G_{ij}(\boldsymbol{x}, \boldsymbol{x}_0) = \frac{\delta_{ij}}{r} + \frac{\hat{x}_i \hat{x}_j}{r^3}, \quad T_{ijk}(\boldsymbol{x}, \boldsymbol{x}_0) = -6\frac{\hat{x}_i \hat{x}_j \hat{x}_k}{r^5}, \tag{2.4}$$

are the free-space Green's function and associated stress tensors, $\hat{\boldsymbol{x}} = \boldsymbol{x} - \boldsymbol{x}_0$, $r = |\hat{\boldsymbol{x}}|$, and δ_{ij} is Kronecker's delta (e.g. Pozrikidis 1992). Note that the integral representation (2.2) involves the total traction over the particle surface and the disturbance traction over the wall and film surface. To formulate the total traction, we have used the reciprocal identity for the unperturbed parabolic flow over the particle volume. Over the free-surface located at $x = h$, the unit normal vector is in the $-x$-direction, the x velocity component is zero, and the double-layer potential takes the form

$$\mathscr{D}_j(\boldsymbol{x}_0, \boldsymbol{u}, F) = 6\hat{x} \iint_F \frac{u_x \hat{x} + u_y \hat{y} + u_z \hat{z}}{[(h - x_0)^2 + \hat{y}^2 + \hat{z}^2]^{5/2}} (\boldsymbol{x} - \boldsymbol{x}_0)_j \, \mathrm{d}S(\boldsymbol{x})$$

$$= 6\hat{x} \iint_F \frac{u_x \hat{x} + u_\sigma (\sigma - \sigma_0 \cos\hat{\varphi}) + u_\varphi \sigma_0 \sin\hat{\varphi}}{(\hat{x}^2 + \sigma^2 + \sigma_0^2 - 2\sigma\sigma_0 \cos\hat{\varphi})^{5/2}} (\boldsymbol{x} - \boldsymbol{x}_0)_j \, \mathrm{d}S(\boldsymbol{x}), \quad (2.5)$$

where $\hat{x} = h - x_0$, φ is the meridional angle, $\hat{\varphi} = \varphi - \varphi_0$, and σ is the distance from the x-axis defined in figure 1. The associated cylindrical polar components are

$$\begin{bmatrix} \mathscr{D}_x \\ \mathscr{D}_\sigma \\ \mathscr{D}_\varphi \end{bmatrix} (\boldsymbol{x}_0, \boldsymbol{u}, F) = 6\hat{x} \iint_F \frac{u_x \hat{x} + u_\sigma (\sigma - \sigma_0 \cos\hat{\varphi}) + u_\varphi \sigma_0 \sin\hat{\varphi}}{(\hat{x}^2 + \sigma^2 + \sigma_0^2 - 2\sigma\sigma_0 \cos\hat{\varphi})^{5/2}} \begin{bmatrix} \hat{x} \\ \sigma \cos\hat{\varphi} - \sigma_0 \\ \sigma \sin\hat{\varphi} \end{bmatrix} \mathrm{d}S(\boldsymbol{x}). \quad (2.6)$$

Applying (2.2) over the wall and requiring the zero-velocity boundary condition, we find

$$\mathscr{S}(\boldsymbol{x}_0, \boldsymbol{f}, P) + \mathscr{S}(\boldsymbol{x}_0, \boldsymbol{f}^D, WF) - \mu \mathscr{D}(\boldsymbol{x}_0, \boldsymbol{u}^D, F) = \boldsymbol{0}, \quad (2.7)$$

where the point $\boldsymbol{x}_0$ lies on W. Applying (2.2) over the particle surface and using the rigid-body-motion boundary condition, we find

$$\mathscr{S}(\boldsymbol{x}_0, \boldsymbol{f}, P) + \mathscr{S}(\boldsymbol{x}_0, \boldsymbol{f}^D, WF) - \mu \mathscr{D}(\boldsymbol{x}_0, \boldsymbol{u}^D, F) = -8\pi\mu [\boldsymbol{V} + \boldsymbol{\Omega} \times (\boldsymbol{x}_0 - \boldsymbol{x}_c) - \boldsymbol{u}^\infty], \quad (2.8)$$

where the point $\boldsymbol{x}_0$ lies on P. Finally applying (2.2) over the film surface and noting that the principal value of the double-layer potential is identically zero due to vanishing of the kernel, T_{ijk}, we find

$$\mathscr{S}(\boldsymbol{x}_0, \boldsymbol{f}, P) + \mathscr{S}(\boldsymbol{x}_0, \boldsymbol{f}^D, WF) + 4\pi\mu \boldsymbol{u}^D(\boldsymbol{x}_0) = \boldsymbol{0}, \quad (2.9)$$

where the point $\boldsymbol{x}_0$ lies on F. The last three equations provide us with a system of nine scalar equations for the three components of the traction over the particle, the three components of the disturbance traction over the wall, the normal component of the traction over the film surface, and the two tangential components of the disturbance velocity over the film surface. This three-dimensional problem presents us with significant numerical challenges concerning the discretization of the three surfaces bounding the flow and the accurate evaluation of the singular boundary integrals.

A key observation is that, because the free-surface is assumed to be virtually flat, the boundaries of the flow, but not the flow itself, are axially symmetric with respect to the x-axis. This geometrical property allows us to simplify the problem by expressing the cylindrical polar components of the left- and right-hand sides of (2.7)–(2.9) in Fourier series with respect to the meridional angle, φ, defined such that $y = \sigma \cos\varphi$ and $z = \sigma \sin\varphi$. Since we are interested in a particle that is freely convected in the film flow, we set V_x, V_z, Ω_x, and Ω_y to zero, and obtain

$$\boldsymbol{V} + \boldsymbol{\Omega} \times (\boldsymbol{x} - \boldsymbol{x}_c) - \boldsymbol{u}^\infty = -\Omega_z \sigma \cos\varphi \, \boldsymbol{e}_x + W(x) \cos\varphi \, \boldsymbol{e}_\sigma - W(x) \sin\varphi \, \boldsymbol{e}_\varphi, \quad (2.10)$$

where $\boldsymbol{e}_x$, $\boldsymbol{e}_\sigma$, $\boldsymbol{e}_\varphi$, are unit vectors, $W(x) = V_y + \Omega_z \tilde{x} - u_y^\infty(x)$, and $\tilde{x} = x - x_c$. Motivated by this form, we express the velocity as

$$\boldsymbol{u} = \mathscr{V}_x \cos\varphi \boldsymbol{e}_x + \mathscr{V}_\sigma \cos\varphi \boldsymbol{e}_\sigma - \mathscr{V}_\varphi \sin\varphi \boldsymbol{e}_\varphi, \tag{2.11}$$

and the boundary traction as

$$\boldsymbol{f} = \mathscr{F}_x \cos\varphi\, \boldsymbol{e}_x + \mathscr{F}_\sigma \cos\varphi\, \boldsymbol{e}_\sigma - \mathscr{F}_\varphi \sin\varphi\, \boldsymbol{e}_\varphi, \tag{2.12}$$

where the coefficients $\mathscr{V}_\alpha$ and $\mathscr{F}_\alpha$ are functions of x and σ. The y component of the force and the z component of the torque exerted on the particle are given by

$$F_y = \pi \int_C (\mathscr{F}_\sigma + \mathscr{F}_\varphi)\, \sigma \, \mathrm{d}l, \quad T_z = \pi \int_C (\tilde{x}\,(\mathscr{F}_\sigma + \mathscr{F}_\varphi) - \sigma\, \mathscr{F}_x)\, \sigma \, \mathrm{d}l, \tag{2.13}$$

where C is the particle contour in the $\varphi = 0$ azimuthal plane consisting of half the (x, y)-plane, and l is the arclength along C. All other components of the force and torque are zero.

Substituting (2.12) in the x component of the single-layer potential and collecting similar terms, we find

$$\begin{aligned}\mathscr{S}_x(\boldsymbol{x}_0) &= \int_C \int_0^{2\pi} (\mathscr{F}_x \cos\varphi\, G_{xx} + (\mathscr{F}_\sigma \cos^2\varphi + \mathscr{F}_\varphi \sin^2\varphi)\, G_{yx} \\ &\quad + (\mathscr{F}_\sigma - \mathscr{F}_\varphi) \sin\varphi \cos\varphi\, G_{zx})\, \mathrm{d}\varphi\, \sigma\, \mathrm{d}l \\ &= \cos\varphi_0 \int_C (\Psi_{xx}\mathscr{F}_x + \Psi_{x\sigma}\mathscr{F}_\sigma + \Psi_{x\varphi}\mathscr{F}_\varphi)\, \mathrm{d}l, \end{aligned} \tag{2.14}$$

where $\Psi_{\alpha\beta}$ are derived kernels. Working in a similar fashion with the other components, we find

$$\begin{bmatrix} \mathscr{S}_x \\ \mathscr{S}_\sigma \\ \mathscr{S}_\varphi \end{bmatrix} (\boldsymbol{x}_0) = \int_C \begin{bmatrix} \cos\varphi_0(\Psi_{xx}\mathscr{F}_x + \Psi_{x\sigma}\mathscr{F}_\sigma + \Psi_{x\varphi}\mathscr{F}_\varphi) \\ \cos\varphi_0(\Psi_{\sigma x}\mathscr{F}_x + \Psi_{\sigma\sigma}\mathscr{F}_\sigma + \Psi_{\sigma\varphi}\mathscr{F}_\varphi) \\ -\sin\varphi_0(\Psi_{\varphi x}\mathscr{F}_x + \Psi_{\varphi\sigma}\mathscr{F}_\sigma + \Psi_{\varphi\varphi}\mathscr{F}_\varphi) \end{bmatrix} \mathrm{d}l. \tag{2.15}$$

Straightforward algebra yields the 3×3 kernel matrix

$$\Psi_{\alpha\gamma}(\boldsymbol{x}_0, \boldsymbol{x}) = \sigma \begin{bmatrix} \mathscr{I}_{11} + \hat{x}^2\mathscr{I}_{31} & \hat{x}(\sigma\,\mathscr{I}_{31} - \sigma_0\mathscr{I}_{32}) \\ \hat{x}(\sigma\,\mathscr{I}_{32} - \sigma_0\mathscr{I}_{31}) & \mathscr{I}_{12} + (\sigma^2 + \sigma_0^2)\mathscr{I}_{32} - \sigma\sigma_0\,(\mathscr{I}_{33} + \mathscr{I}_{31}) \\ \hat{x}\sigma(\mathscr{I}_{30} - \mathscr{I}_{32}) & \mathscr{I}_{10} - \mathscr{I}_{12} + \sigma^2(\mathscr{I}_{30} - \mathscr{I}_{32}) - \sigma\sigma_0\,(\mathscr{I}_{31} - \mathscr{I}_{33}) \end{bmatrix}$$

$$\begin{bmatrix} \hat{x}\sigma_0(\mathscr{I}_{32} - \mathscr{I}_{30}) \\ \mathscr{I}_{10} - \mathscr{I}_{12} + \sigma_0^2\,(\mathscr{I}_{30} - \mathscr{I}_{32}) \\ \hat{x}\sigma(\mathscr{I}_{30} - \mathscr{I}_{32})\mathscr{I}_{12} + \sigma\sigma_0(\mathscr{I}_{31} - \mathscr{I}_{33}) \end{bmatrix}, \tag{2.16}$$

where

$$\mathscr{I}_{mn} = \int_0^{2\pi} \frac{\cos^n\omega\, \mathrm{d}\omega}{\left[\hat{x}^2 + \sigma^2 + \sigma_0^2 - 2\sigma\sigma_0\cos\omega\right]^{m/2}} = \frac{4w^m}{(4\sigma\sigma_0)^{m/2}} \int_0^{\pi/2} \frac{(2\cos^2\omega - 1)^n}{(1 - w^2\cos^2\omega)^{m/2}} \mathrm{d}\omega, \tag{2.17}$$

and $w^2 = 4\sigma\sigma_0/[\hat{x}^2 + (\sigma + \sigma_0)^2]$. These integrals may be expressed in terms of complete elliptic integrals of the first and second kind, which may be evaluated efficiently either by library functions or by iterative methods.

Next, we substitute (2.11) in the double-layer potential (2.6) and work in a similar fashion to obtain

$$\begin{bmatrix} \mathscr{D}_x \\ \mathscr{D}_\sigma \\ \mathscr{D}_\varphi \end{bmatrix} (\boldsymbol{x}_0) = \int_C \begin{bmatrix} \cos\varphi_0 (K_{xx} \mathscr{V}_x + K_{x\sigma} \mathscr{V}_\sigma + K_{x\varphi} \mathscr{V}_\varphi) \\ \cos\varphi_0 (K_{\sigma x} \mathscr{V}_x + K_{\sigma\sigma} \mathscr{V}_\sigma + K_{\sigma\varphi} \mathscr{V}_\varphi) \\ -\sin\varphi_0 (K_{\varphi x} \mathscr{V}_x + K_{\varphi\sigma} \mathscr{V}_\sigma + K_{\varphi\varphi} \mathscr{V}_\varphi) \end{bmatrix} \mathrm{d}l. \tag{2.18}$$

Straightforward algebra yields the 3×3 kernel matrix

$$K_{\alpha\beta}(\boldsymbol{x}_0, \boldsymbol{x}) = 6\sigma\hat{x} \begin{bmatrix} \hat{x}^2 \mathscr{I}_{51} & \hat{x}(\sigma \mathscr{I}_{51} - \sigma_0 \mathscr{I}_{52}) & \hat{x}\sigma_0 (\mathscr{I}_{52} - \mathscr{I}_{50}) \\ \hat{x}(\sigma \mathscr{I}_{52} - \sigma_0 \mathscr{I}_{51}) & (\sigma^2 + \sigma_0^2) \mathscr{I}_{52} - \sigma\sigma_0 (\mathscr{I}_{51} + \mathscr{I}_{53}) & \sigma\sigma_0 (\mathscr{I}_{53} - \mathscr{I}_{51}) - \sigma_0^2 (\mathscr{I}_{52} - \mathscr{I}_{50}) \\ \hat{x}\sigma (\mathscr{I}_{50} - \mathscr{I}_{52}) & \sigma^2 (\mathscr{I}_{50} - \mathscr{I}_{52}) + \sigma\sigma_0 (\mathscr{I}_{53} - \mathscr{I}_{51}) & \sigma\sigma_0 (\mathscr{I}_{51} - \mathscr{I}_{53}) \end{bmatrix}. \tag{2.19}$$

Substituting these expressions in (2.2), we derive an integral representation for the Fourier coefficients,

$$\mathscr{V}_\alpha^D(\boldsymbol{x}_0) = -\frac{1}{8\pi\mu} \int_{C_P} \Psi_{\alpha\beta}(\boldsymbol{x}_0, \boldsymbol{x}) \mathscr{F}_\beta(\boldsymbol{x}) \, \mathrm{d}l(\boldsymbol{x}) - \frac{1}{8\pi\mu} \int_{C_{WF}} \Psi_{\alpha\beta}(\boldsymbol{x}_0, \boldsymbol{x}) \mathscr{F}_\beta^D(\boldsymbol{x}) \, \mathrm{d}l(\boldsymbol{x}) + \frac{1}{8\pi} \int_{C_F} K_{\alpha\delta}(\boldsymbol{x}_0, \boldsymbol{x}) \mathscr{V}_\delta^D(\boldsymbol{x}) \, \mathrm{d}l(\boldsymbol{x}), \tag{2.20}$$

where the point $\boldsymbol{x}_0$ lies inside the film and δ runs over σ and φ. Substituting in (2.7), we obtain the one-dimensional integral equation

$$\int_{C_P} \Psi_{\alpha\beta}(\boldsymbol{x}_0, \boldsymbol{x}) \mathscr{F}_\beta(\boldsymbol{x}) \, \mathrm{d}l(\boldsymbol{x}) + \int_{C_{WF}} \Psi_{\alpha\beta}(\boldsymbol{x}_0, \boldsymbol{x}) \mathscr{F}_\beta^D(\boldsymbol{x}) \, \mathrm{d}l(\boldsymbol{x}) - \mu \int_{C_F} K_{\alpha\delta}(\boldsymbol{x}_0, \boldsymbol{x}) \mathscr{V}_\delta^D(\boldsymbol{x}) \, \mathrm{d}l(\boldsymbol{x}) = 0, \tag{2.21}$$

where the point $\boldsymbol{x}_0$ lies on W. Substituting in (2.8), we obtain

$$\int_{C_P} \Psi_{\alpha\beta}(\boldsymbol{x}_0, \boldsymbol{x}) \mathscr{F}_\beta(\boldsymbol{x}) \, \mathrm{d}l(\boldsymbol{x}) + \int_{C_{WF}} \Psi_{\alpha\beta}(\boldsymbol{x}_0, \boldsymbol{x}) \mathscr{F}_\beta^D(\boldsymbol{x}) \, \mathrm{d}l(\boldsymbol{x}) - \mu \int_{C_F} K_{\alpha\delta}(\boldsymbol{x}_0, \boldsymbol{x}) \mathscr{V}_\delta^D(\boldsymbol{x}) \, \mathrm{d}l(\boldsymbol{x}) = -8\pi\mu(-\Omega_z \sigma_0 \delta_{\alpha x} + W(\boldsymbol{x}_0) \delta_{\alpha\sigma} + W(\boldsymbol{x}_0) \delta_{\alpha\varphi}), \tag{2.22}$$

where the point $\boldsymbol{x}_0$ lies on P. Finally substituting in (2.9), we find

$$\int_{C_P} \Psi_{\alpha\beta}(\boldsymbol{x}_0, \boldsymbol{x}) \mathscr{F}_\beta(\boldsymbol{x}) \, \mathrm{d}l(\boldsymbol{x}) + \int_{C_{WF}} \Psi_{\alpha\beta}(\boldsymbol{x}_0, \boldsymbol{x}) \mathscr{F}_\beta^D(\boldsymbol{x}) \, \mathrm{d}l(\boldsymbol{x}) + 4\pi\mu \mathscr{V}_\alpha^D(\boldsymbol{x}_0) = 0, \tag{2.23}$$

where the point $\boldsymbol{x}_0$ lies on the free-surface, F. The boundary conditions require $\mathscr{F}_\sigma^D = 0$, $\mathscr{F}_\varphi^D = 0$ and $\mathscr{V}_x^D = 0$ over F.

The solution for the x component of the disturbance traction, which is equal to the total traction over the free surface, can be used to deduce the surface deformation to leading order with respect to the Bond number, $Bo = \mu U_s / \gamma$. If the free-surface is described as $x = h\,[1 + Bo\,\phi(y, z)] = h\,[1 + Bo \cos\varphi\, \Phi(\sigma)]$, then a perturbation expansion with respect to Bo shows that, to zeroth order, $f_x \simeq -\mu U_s h \nabla^2 \phi$, where ϕ and Φ are dimensionless functions and ∇^2 is the two-dimensional Laplacian written

with respect to y and z. Making substitutions, we derive the inhomogeneous Bessel-like ordinary differential equation

$$\frac{1}{\sigma}\frac{\mathrm{d}}{\mathrm{d}\sigma}\left(\sigma\,\frac{\mathrm{d}\Phi}{\mathrm{d}\sigma}\right)-\frac{\Phi}{\sigma^2}=\frac{\mathrm{d}}{\mathrm{d}\sigma}\left(\frac{1}{\sigma}\frac{\mathrm{d}(\sigma\Phi)}{\mathrm{d}\sigma}\right)=-\frac{\mathscr{F}_x}{\mu U_s h}, \tag{2.24}$$

where the right-hand side is known in numerical form. A similar approach has been pursued by previous authors to compute the small deformation of the interface between viscous fluids due to a perturbation (e.g. Aderogba & Blake 1978).

To solve the integral equations, we divide the boundary contours in the $\varphi=0$ meridional plane into straight elements over the wall and free-surface and circular elements over the particle, and approximate the Fourier coefficients by constant functions over each element. For better accuracy, the elements are concentrated near the axis of symmetry so that their length increases geometrically with respect to arclength, as shown in figure 2(*a*). The ratio of the sizes of the mid-point element and end-point element over the particle was set to 10; the element stretch ratio on the wall and free-surface elements was then determined so that particle, wall, and surface elements adjacent to the axis of revolution have equal lengths. The wall and free-surface contours were truncated at a radial distance equal to $10h$. Applying point collocation at the mid-point of each element, we derive a system of linear equations for the unknown solution vector:

$$\left[(\mathscr{F}_x)_P\ \left(\mathscr{F}_x^D\right)_W\ \left(\mathscr{F}_x^D\right)_F\,\middle|\,(\mathscr{F}_\sigma)_P\ \left(\mathscr{F}_\sigma^D\right)_W\ \left(\mathscr{V}_\sigma^D\right)_F\,\middle|\,(\mathscr{F}_\varphi)_P\ \left(\mathscr{F}_\varphi^D\right)_W\ \left(\mathscr{V}_\varphi^D\right)_F\right], \tag{2.25}$$

where the vector block $(\mathscr{F}_x)_P$ contains the x component of the traction over all wall elements; the rest of the blocks are defined in similar ways. For a freely suspended particle, the translational and angular velocities V_y and Ω_z are appended to the vector of unknowns, and two more equations are introduced expressing the vanishing of the force and torque, F_y and T_z. The influence coefficients over the non-singular elements are computed by the six-point Gauss–Legendre quadrature. The diagonal components of the dimensionless single-layer kernel, $\Psi_{\alpha\alpha}$, exhibit a logarithmic singularity as the azimuthal angle of the integration point, θ, tends to the azimuthal angle of the evaluation point, θ_0, $\Psi_{xx}\simeq -2\log|\theta-\theta_0|$, $\Psi_{\varphi\varphi}\simeq -2\log|\theta-\theta_0|$, $\Psi_{\varphi\varphi}\simeq -4\log|\theta-\theta_0|$. These singularities are subtracted out and integrated analytically following the numerical quadrature. The solution of the ordinary differential equation (2.24) was found by a standard finite volume method subject to a regularity condition at the axis and the condition of zero slope at the truncated end of the wall contour.

3. Results and discussion

Figure 2(*b–d*) shows the distribution of the traction along the particle contour, the distribution of the disturbance traction along the wall, and the distribution of the disturbance traction and velocity along the free-surface for $a/h=0.25$ and $x_c/h=0.30$. The traction coefficients have been scaled by $\mu U_s/h$, and the velocity coefficients have been scaled by U_s. The solid lines representing the x Fourier coefficient of the traction tend to zero at the axis of symmetry in all graphs, while the corresponding σ and φ coefficients of the traction and velocity tend to common values. This ensures that the solution is single valued at the x-axis. The results show that the perturbation traction decays much faster than the perturbation velocity over the free-surface. Figure 2(*e*) illustrates the disturbance velocity vector field over the free-surface. When the y velocity of the Nusselt flow is added to this pattern, we obtain an overwhelming unidirectional surface flow. Figure 2(*f*) illustrates the deformation

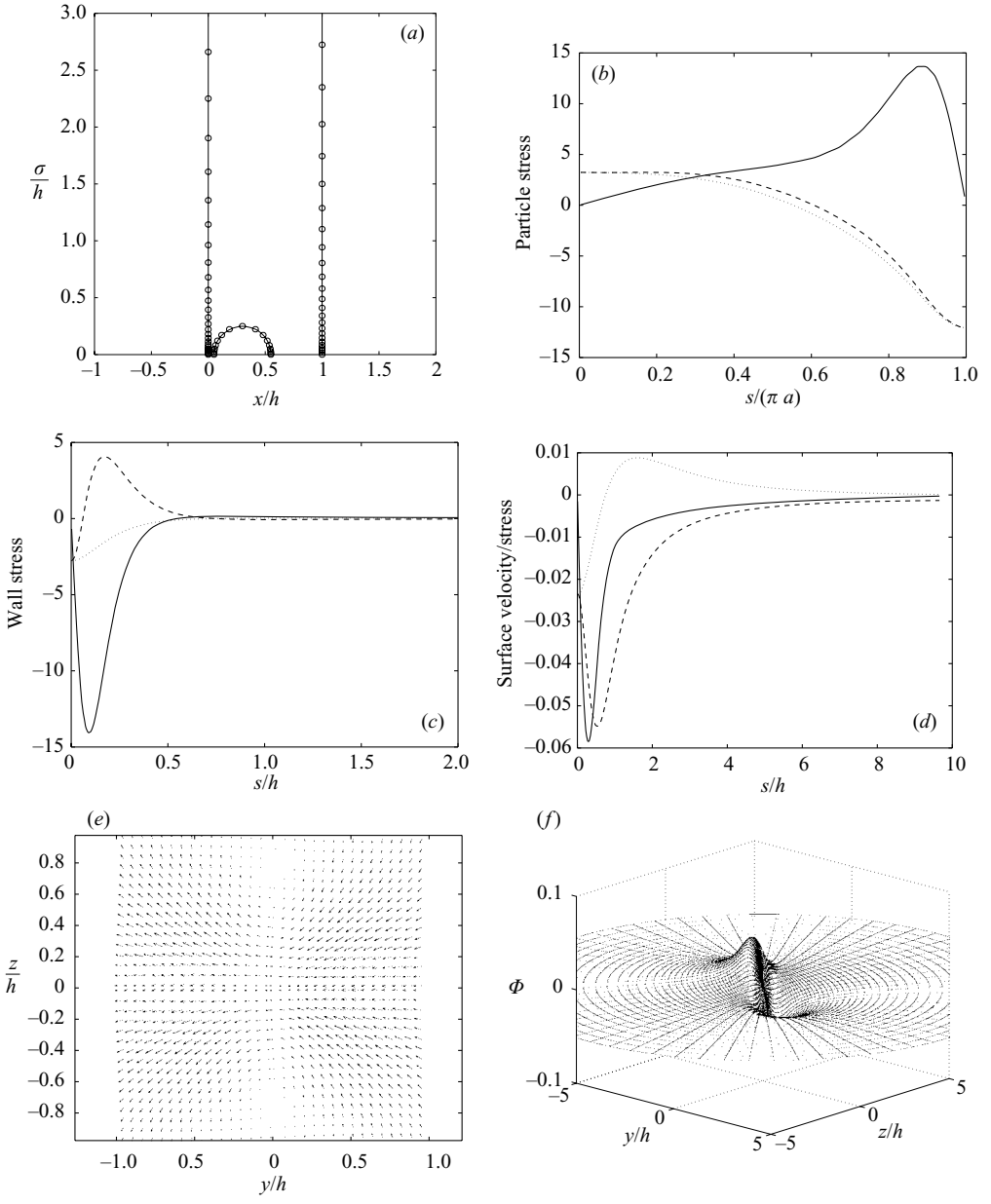

FIGURE 2. (*a*) Sample boundary element grid for $a/h = 0.25$ and $x_c/h = 0.30$ showing the high density near the axis of revolution. (*b*) Distribution of the scaled particle traction coefficients $\mathscr{F}_x$ (solid line), $\mathscr{F}_\sigma$ (dashed line), $\mathscr{F}_\varphi$ (dotted line), and (*c*) distribution of the scaled disturbance wall traction coefficients $\mathscr{F}_x^D$ (solid line), $\mathscr{F}_\sigma^D$ (dashed line), $\mathscr{F}_\varphi^D$ (dotted line), plotted with respect to arclength, s, measured from the axis of revolution. (*d*) Distribution of the scaled surface traction coefficient $\frac{1}{10}\mathscr{F}_x^D$ (solid line), and velocity coefficients $\mathscr{V}_\sigma^D$ (dashed line), $\mathscr{V}_\varphi^D$ (dotted line), plotted with respect to arclength measured from the axis of symmetry. (*e*) Disturbance velocity vector field over the free surface, and (*e*) deformed shape of the free surface.

	x_c/h	0.0564	0.10	0.20	0.30	0.40	0.50	0.60	0.70	0.80	0.90
$a/h=0.05$	V_y/U_y^∞	0.765 (0.767)	0.962	0.994	0.997	0.998	0.999	0.999	0.999	0.999	0.999
	$2\Omega_z/\omega_z^\infty$	0.781 (0.780)	0.965	0.995	0.999	0.999	1.000	0.999	0.999	0.995	0.962
	x_c/h	0.1691	0.20	0.30	0.40	0.50	0.60	0.70	0.80	0.825	
$a/h=0.15$	V_y/U_y^∞	0.762 (0.767)	0.869	0.958	0.978	0.986	0.989	0.991	0.991	0.991	
	$2\Omega_z/\omega_z^\infty$	0.786 (0.780)	0.884	0.965	0.982	0.986	0.981	0.961	0.871	0.800	
	x_c/h	0.275	0.30	0.40	0.50	0.60	0.70	0.725			
$a/h=0.25$	V_y/U_y^∞	0.735	0.813	0.920	0.951	0.964	0.969	0.969			
	$2\Omega_z/\omega_z^\infty$	0.764	0.832	0.921	0.935	0.912	0.811	0.743			
	x_c/h	0.375	0.40	0.50	0.60	0.625					
$a/h=0.35$	V_y/U_y^∞	0.697	0.771	0.880	0.915	0.918					
	$2\Omega_z/\omega_z^\infty$	0.709	0.766	0.820	0.744	0.685					
	x_c/h	0.475	0.50	0.525							
$a/h=0.45$	V_y/U_y^∞	0.652	0.722	0.762							
	$2\Omega_z/\omega_z^\infty$	0.571	0.592	0.571							

TABLE 1. Translational and angular velocities of a freely suspended particle in film flow, as functions of the particle radius and distance of the particle centre from the wall. The entries in parentheses are the predictions of Goldman *et al.* (1967) for a spherical particle suspended in a semi-infinite simple shear flow above a plane wall.

of the free-surface computed by solving a Bessel-like equation, as discussed in the previous section. We observe the formation of a peak and a depression upstream and downstream of the particle centre along the y-axis. These results are useful for quantifying the rippling of a free-surface in the flow of a suspension.

Table 1 lists the computed particle translational and angular velocities scaled, respectively, by the fluid velocity and half the vorticity of the Nusselt profile evaluated at the particle centre. Results are presented for several combinations of the particle radius and particle centre position, with a margin of error of less than ± 0.001 in all cases. For $a/h=0.25$ and $x_c/h=0.30$, computations with triplets of elements (16, 32, 32), (32, 64, 64), and (64, 128, 128), around the particle, wall, and free-surface contour, yielded, respectively, $V_y/U_y^\infty=0.8141$, 0.8130, 0.8128, and $2\Omega_z/\omega_z^\infty=0.8342$, 0.8326, 0.8322. These data demonstrate the fast convergence and good accuracy of the numerical method even with a moderate number of elements. All results reported in the table were obtained with the finest grid. In all cases, the reduced translational velocity is less than unity, reflecting a lag in the particle velocity with respect to the pure fluid velocity due to the finite particle size. For a fixed particle radius, V_y/U_y^∞ increases monotonically toward the value of unity as the particle centre moves away from the wall and toward the free-surface. In contrast, the reduced angular velocity $2\Omega_z/\omega_z^\infty$ increases up to a maximum, and then declines toward a finite limit as the particle centre approaches the free-surface where the vorticity of the unperturbed flow vanishes. For a fixed particle centre, both reduced velocities decline as the particle radius is increased. The predictions of Goldman, Cox & Brenner (1967) for a spherical particle suspended in a semi-infinite simple shear flow are enclosed by parentheses in table 1. These theoretical estimates are in excellent agreement with the numerical results for small particles that are close enough to the wall.

Next, we consider flow past an immobilized particle, set the particle translational and angular velocities equal to zero, and compute the force and torque exerted on the particle as part of the solution. Figure 3(*a–c*) shows the distribution of the traction over the particle contour, the distribution of the disturbance traction over the wall, and the distribution of the disturbance traction and velocity along the surface for

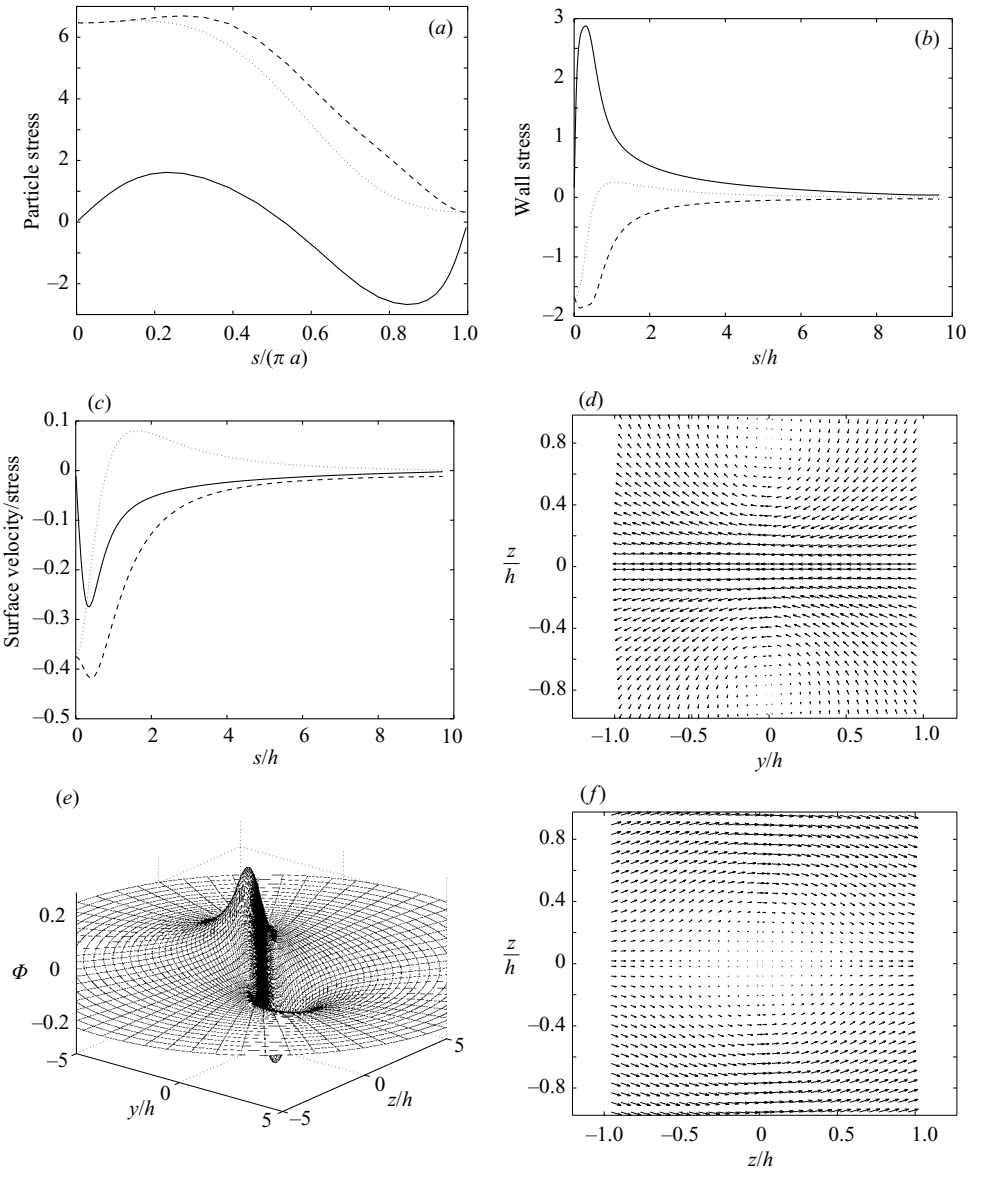

FIGURE 3. Flow past an immobilized particle of radius $a/h = 0.35$ placed at a distance $x_c/a = 1.0453$ above a plane wall. Frames (a–e) are the counterparts of those shown in figure 2(b–f). (f) Total velocity vector field for a large particle with $a/h = 0.475$ and $x_c/a = 1.0453$.

$a/h = 0.35$ and $x_c/a = 1.0453$. The traction coefficients have been scaled by $\mu U_s/h$, and the velocity coefficients have been scaled by U_s. Comparing these graphs with their counterparts for a freely suspended particle shown in figure 2(b–d), we find significant differences over the particle surface and wall, and a similar behavior over the free-surface. The surface velocity vector field and surface deformation illustrated in figure 3(d, e) are generally similar to those induced by a freely suspended particle, though the surface deformation is much more pronounced. Figure 3(f) shows the total velocity vector field for a large particle with $a/h = 0.475$ and $x_c/a = 1.0453$. In

a/h	0.0	0.05	0.15	0.25	0.35	0.40	0.45	0.475
$F_y/(6\pi\mu a x_c S)$	1.668	1.710	1.838	2.039	2.275	2.378	2.458	2.492
$T_z/(4\pi\mu a^3 S)$	0.947	0.947	0.955	0.953	0.850	0.708	0.472	0.319

TABLE 2. Force and torque exerted on a spherical particle held stationary at a distance $x_c/a = 1.0453$ above the inclined wall; S is the shear rate of the unidirectional Nusselt flow evaluated at the particle centre.

this case, we observe a region of expansion as the fluid negotiates the nearby upper particle surface.

Table 2 lists the force and torque exerted on an immobilized particle that nearly touches the wall. The theoretical predictions of Goldman *et al.* (1967) for a spherical particle held stationary in semi-infinite simple shear flow, listed under the zero radius header, are in excellent agreement with the numerical results for small particles. As the particle becomes larger, the force coefficient increases monotonically, while the torque coefficient reaches a maximum and then decreases toward a non-zero limit. The results presented in table 2 are useful for estimating the critical adhesion force and torque required for a particle to remain attached to the wall.

This research was supported by a grant provided by the National Science Foundation.

REFERENCES

ADEROGBA, K. & BLAKE, J. R. 1978 Action of a force near the planar interface between semi-infinite immiscible liquids at very low Reynolds numbers. *Bull. Austral. Math. Soc.* **18**, 345–356, Addendum: **19**, 309–318.

BLYTH, M. G. & POZRIKIDIS, C. 2006 Film flow down an inclined plane over a three-dimensional obstacle. *Phys. Fluids* **18**, 051706.

GOLDMAN, A. J., COX, R. G. & BRENNER, H. 1967 Slow viscous motion of a sphere parallel to a plane wall. Part II: Couette flow. *Chem. Engng Sci.* **22**, 653–660.

LI, X. & POZRIKIDIS, C. 2002 Film flow of a suspension of liquid drops. *Phys. Fluids* **14**, 61–74.

LI, X. & POZRIKIDIS, C. 2003 Film flow of a suspension down an inclined plane. *Phil. Trans. R. Soc. Lond.* A **361**, 847–869.

LOIMER, T., NIR, A. & SEMIAT, R. 2002 Shear-induced corrugation of free interfaces in concentrated suspensions. *J. Non-Newtonian Fluid Mech.* **102**, 115–134.

MATZEN, G. W. 1997 Effect of microscale protrusions in local fluid flow and mass transport in the presence of forced convection. Doctoral Dissertation in Chemical Engineering, Univ. California, Berkeley.

POZRIKIDIS, C. 1992 *Boundary Integral and Singularity Methods for Linearized Viscous Flow*. Cambridge University Press.

POZRIKIDIS, C. 1994*a* The motion of particles in the Hele-Shaw cell. *J. Fluid Mech.* **261**, 199–222.

POZRIKIDIS, C. 1994*b* Shear flow over a plane wall with an axisymmetric cavity or a circular orifice of finite thickness. *Phys. Fluids* **6**, 68–79.

POZRIKIDIS, C. 1997 Shear flow over a protuberance on a plane wall. *J. Engng Maths* **31**, 31–44.

POZRIKIDIS, C. 2000 Effect of pressure gradient on viscous shear ow past an axisymmetric depression or protuberance on a plane wall. *Computers Fluids* **29**, 617–637.

SHATZ, L. 2004 Indirect boundary element method for unsteady linearized flow over prolate and oblate spheroids and hemispheroidal protuberances. *Intl. J. Numer. Meth. Fluids* **44**, 147–174.

SINGH, A., NIR, A. & SEMIAT, R. 2006 Free-surface flow of concentrated suspensions. *Intl J. Multiphase Flow* (In Press).

TIMBERLAKE, B. D. & MORRIS, J. F. 2005 Particle migration and free-surface topography in inclined plane flow of a suspension. *J. Fluid Mech.* **538**, 309–341.